Mechanisms behind large Gilbert damping anisotropies

I. P. Miranda [1], A. B. Klautau [2,*] A. Bergman,[3] D. Thonig,[3,4] H. M. Petrilli [1], and O. Eriksson [3,4]

[1]*Universidade de São Paulo, Instituto de Física, Rua do Matão, 1371, 05508-090, São Paulo, SP, Brazil*
[2]*Faculdade de Física, Universidade Federal do Pará, Belém, PA, Brazil*
[3]*Department of Physics and Astronomy, Uppsala University, Box 516, SE-75120 Uppsala, Sweden*
[4]*School of Science and Technology, Örebro University, Fakultetsgatan 1, SE-701 82 Örebro, Sweden*

A method with which to calculate the Gilbert damping parameter from a real-space electronic structure method is reported here. The anisotropy of the Gilbert damping with respect to the magnetic moment direction and local chemical environment is calculated for bulk and surfaces of $Fe_{50}Co_{50}$ alloys from first-principles electronic structure in a real-space formulation. The size of the damping anisotropy for $Fe_{50}Co_{50}$ alloys is demonstrated to be significant. Depending on details of the simulations, it reaches a maximum-minimum damping ratio as high as 200%. Several microscopic origins of the strongly enhanced Gilbert damping anisotropy have been examined, where in particular interface/surface effects stand out, as do local distortions of the crystal structure. Although theory does not reproduce the experimentally reported high ratio of 400% [Phys. Rev. Lett. **122**, 117203 (2019)], it nevertheless identifies microscopic mechanisms that can lead to huge damping anisotropies.

Introduction. Magnetic damping has a critical importance in determining the lifetime, diffusion, transport, and stability of domain walls, magnetic vortices, skyrmions, and any nanoscale complex magnetic configurations [1]. Given its high scientific interest, a possibility to obtain this quantity by means of first-principles theory [2] opens new perspectives of finding and optimizing materials for spintronic and magnonic devices [3–8]. Among the more promising ferromagnets to be used in spintronics devices, cobalt-iron alloys demonstrate high potentials due to the combination of ultralow damping with metallic conductivity [4,9].

Recently, Li *et al.* [10] reported an observed, giant anisotropy of the Gilbert damping (α) in epitaxial $Fe_{50}Co_{50}$ thin films (with thickness of $10 - 20$ nm) reaching maximum-minimum damping ratio values as high as 400%. The authors of Ref. [10] claimed that the observed effect is likely due to changes in the spin-orbit coupling (SOC) influence for different crystalline directions caused by short-range orderings that lead to local structural distortions. This behavior differs distinctly from, for example, pure bcc Fe [11]. In order to quantitatively predict the Gilbert damping, Kambersky's breathing Fermi surface (BFS) [12] and torque-correlation (TC) [13] models are frequently used. These methods have been explored for elements and alloys, in bulk form or at surfaces, mostly via reciprocal-space *ab initio* approaches, in a collinear or (more recently) in a noncollinear configuration [14]. However, considering heterogeneous materials, such as alloys with short-range order, and the possibility to investigate element specific, nonlocal contributions to the damping parameter, there are, to the best of our

knowledge, no reports in the literature that rely on a real-space method.

In this Letter, we report on an implementation of *ab initio* damping calculations in a real-space linear muffin-tin orbital method, within the atomic sphere approximation (RS-LMTO-ASA) [15,16], with the local spin-density approximation [17] for the exchange-correlation energy. The implementation is based on the BFS and TC models, and the method (see Supplemental Material for details) is applied to investigate the reported, huge damping anisotropy of $Fe_{50}Co_{50}(100)/MgO$ films [10]. A main result here is the identification of a microscopic origin of the enhanced Gilbert damping anisotropy of $Fe_{50}Co_{50}(100)$ films and the intrinsic relationships to the local geometry of the alloy. Most significantly, we demonstrate that a surface produces extremely large damping anisotropies that can be orders of magnitude larger than those of the bulk. We call attention to the fact that this is the first time, as far as we know, that damping values are theoretically obtained in such a local way.

Results. We calculated: (i) Ordered $Fe_{50}Co_{50}$ in the *B*2 structure (hereafter refereed to as *B*2-FeCo); (ii) random $Fe_{50}Co_{50}$ alloys in bcc or bct structures, where the virtual crystal approximation (VCA) was applied; (iii) $Fe_{50}Co_{50}$ alloys simulated as embedded clusters in a VCA matrix (host). In all cases, VCA was simulated with an electronic concentration corresponding to $Fe_{50}Co_{50}$. The (ii) and (iii) alloys were considered as in bulk as well as in the (001) surface, with bcc and bct structures [hereafter correspondingly refered to as VCA $Fe_{50}Co_{50}$ bcc, VCA $Fe_{50}Co_{50}$ bct, VCA $Fe_{50}Co_{50}(001)$ bcc, and VCA $Fe_{50}Co_{50}(001)$ bct]. The effect of local tetragonal distortions was considered with a local $\frac{c}{a} = 1.09$ ratio (see Supplemental Material for details). All data for cluster based results were obtained from an average of several different configurations. The total damping for a given site i in real space
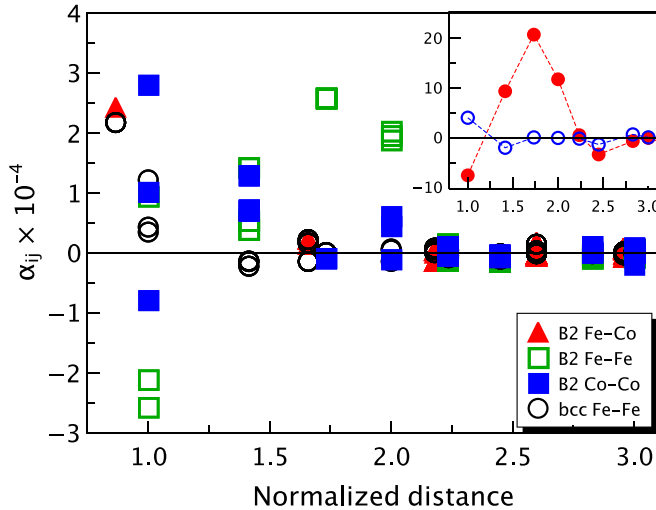
*aklautau@ufpa.br

FIG. 1. Nonlocal damping contributions, α_{ij}, in (Fe-centered) bulk $B2$-FeCo and bcc Fe, as a function of the normalized distance in lattice constant units a. Inset: Nonlocal contributions from only Fe-Fe pairs summed, for each distance, in bcc Fe bulk (empty blue dots) and in the $B2$-FeCo (full red dots). The onsite damping for Fe (Co) in $B2$-FeCo is $\alpha_{\mathrm{onsite}}^{\mathrm{Fe}} = 1.1 \times 10^{-3}$ ($\alpha_{\mathrm{onsite}}^{\mathrm{Co}} = 0.8 \times 10^{-3}$) and for bcc Fe it is $\alpha_{\mathrm{onsite}}^{\mathrm{Fe}} = 1.6 \times 10^{-3}$. The magnetization direction is z ([001]). Lines are guides for the eyes.

[α_t, Eqs. (S6) and (S7)] can be decomposed in nonlocal, α_{ij} ($i \neq j$), and local (onsite), α_{onsite} (or α_{ii}, $i = j$) contributions, each of them described by the tensor elements

$$\alpha_{ij}^{\nu\mu} = \frac{g}{m_i \pi} \int \eta(\epsilon) \mathrm{Tr}\big(\hat{T}_i^{\nu} \mathrm{Im}\hat{G}_{ij} \hat{T}_j^{\mu} \mathrm{Im}\hat{G}_{ji}\big) d\epsilon, \qquad (1)$$

where m_i is the total magnetic moment localized in the reference atomic site i, $\mu, \nu = \{x, y, z\}$, $\hat{T}$ is the torque operator, and $\eta(\epsilon) = \frac{\partial f(\epsilon)}{\partial \epsilon}$ is the derivative of the Fermi distribution. The scalar α_{ij} parameter is defined in the collinear regime as $\alpha_{ij} = \frac{1}{2}(\alpha_{ij}^{xx} + \alpha_{ij}^{yy})$.

To validate our methodology, the here-obtained total damping for several systems (such as bcc Fe, fcc Ni, hcp, and fcc Co and $B2$-FeCo) was compared with established values available in the literature (Supplemental Table S1), where an overall good agreement can be seen.

Figure 1 shows the nonlocal contributions to the damping for bcc Fe and $B2$-FeCo. Although the onsite contributions are around one order of magnitude larger than the nonlocal, there are many α_{ij} to be added and total net values can become comparable. Bcc Fe and $B2$-FeCo have very different nonlocal damping contributions. Element resolved α_{ij} reveals that the summed Fe-Fe interactions dominate over Co-Co for distances until $2a$ in $B2$-FeCo. We observe that α_{ij} is quite extended in space for both bcc Fe and $B2$-FeCo. The different contributions to the nonlocal damping from atoms at equal distance arises from the reduced number of operations in the crystal point group due to the inclusion of SOC in combination with time-reversal symmetry breaking. The $B2$-FeCo arises from replacing every second Fe atom in the bcc structure with a Co atom. It is interesting that this replacement (i.e., the presence of Co in the environment) significantly changes the nonlocal contributions for Fe-Fe pairs, what can more

clearly be seen in the Fig. 1 inset, where the nonlocal damping summed over atoms at the same relative distance for Fe-Fe pairs in bcc Fe and $B2$-FeCo is shown; the nonlocal damping of Fe-Fe pairs is distinctly different for short ranges, while long-ranged (further than $\sim$2.25 Å) contributions are smaller and more isotropic.

The damping anisotropy, i.e., the damping change, when the magnetization is changed from the easy axis to a new direction is

$$\Delta\alpha_t = \left(\frac{\alpha_t^{[110]}}{\alpha_t^{[010]}} - 1\right) \times 100\%, \qquad (2)$$

where $\alpha_t^{[110]}$ and $\alpha_t^{[010]}$ are the total damping obtained for magnetization directions along [110] and [010], respectively; note that this definition is different to the maximum-minimum damping ratio, determined as $\frac{\alpha_t^{[110]}}{\alpha_t^{[010]}} \times 100\%$, from Ref. [10]. Analogous definition also applies for $\Delta\alpha_{\mathrm{onsite}}$. We investigated this anisotropy in surfaces and in bulk systems with (and without) tetragonal structural distortions. Our calculations for VCA Fe$_{50}$Co$_{50}$ bcc show a damping increase of $\sim$13% when changing the magnetization direction from [010] to [110] (Supplemental Table S2). The smallest damping is found for the easy magnetization axis, [010], which holds the largest orbital moment (m_{orb}) [18]. For VCA Fe$_{50}$Co$_{50}$ bcc we obtained a small variation of $\sim$2% for the onsite contribution ($\alpha_{\mathrm{onsite}}^{[010]} = 8.94 \times 10^{-4}$ and $\alpha_{\mathrm{onsite}}^{[110]} = 8.76 \times 10^{-4}$), which implies that the anisotropy comes mostly from the nonlocal contributions, particularly from the next-nearest neighbors. For comparison, $\Delta\alpha_t \sim 3\%$ (with $\Delta\alpha_{\mathrm{onsite}} \sim 0.4\%$) in the case of bcc Fe, which corroborates the reported [11] small bcc Fe anisotropy at room temperature and with the bulk damping anisotropy rates [19].

We also inspected the chemical inhomogeneity influence on the anisotropy, considering the $B2$-FeCo alloy, where the weighted average damping [Eq. (S7)] was used instead. The $B2$-FeCo bcc ($\sim$7%) and VCA Fe$_{50}$Co$_{50}$ bcc ($\sim$13%) anisotropies are of similar magnitudes. Both $B2$ structure and VCA calculations lead to damping anisotropies which are significantly lower than what was observed in the experiments, and it seems likely that the presence of disorder in composition and/or structural properties of the Fe/Co alloy would be important to produce large anisotropy effects on the damping.

We analyzed the role of local distortions by considering a hypothetical case of a large, 15% ($\frac{c}{a} = 1.15$), distortion on the z axis of ordered $B2$-FeCo. We found the largest damping anisotropy ($\sim$24%) when comparing the results with magnetization in the [001] ($\alpha_t^{[001]} = 10.21 \times 10^{-3}$) and in the [010] ($\alpha_t^{[010]} = 7.76 \times 10^{-3}$) directions. This confirms that, indeed, bct-like distortions act in favor of the $\Delta\alpha_t$ enhancement (and therefore, of the maximum-minimum damping ratio), but the theoretical data are not large enough to explain the giant value reported experimentally [10].

Nevertheless, in the case of an alloy, the local lattice distortions suggested in Ref. [10] are most to likely occur in an heterogeneous way [20], with different distortions for different local environments. To inspect this type of influence on the theoretical results, we investigated (Supplemental Table S3) clusters containing different atomic configurations embedded in a VCA Fe$_{50}$Co$_{50}$ matrix (with Fe bulk lattice

TABLE I. Total intralayer damping ($\alpha_t \times 10^{-3}$) and anisotropy, $\Delta\alpha_t$ [Eq. (2)] of a typical (VCA) atom in each $Fe_{50}Co_{50}(001)$ bcc surface layer for magnetization along [010] and [110] directions. In each line, the sum of all α_{ij} in the same layer is considered. Outermost (layer 1) and deeper layers (2–5).

Layer	α_t [010]	α_t [110]	$\Delta\alpha_t$
1	7.00	14.17	+102.4%
2	1.28	1.16	−9.4%
3	2.83	3.30	+16.6%
4	2.18	1.99	−8.7%
5	2.54	2.53	−0.4%

parameter); distortions were also considered such that, locally in the clusters, $\frac{c}{a} = 1.15$ (Supplemental Table S4). Moreover, in both cases, two types of clusters have to be considered: Co-centered and Fe-centered. The α_t was then computed as the sum of the local and nonlocal contributions for clusters with a specific central (Fe or Co) atom, and the average of Fe- and Co-centered clusters was taken. Fe-centered clusters have shown larger anisotropies, on average ∼33% for the undistorted (∼74% for the distorted) compared with ∼8% for the undistorted Co-centered clusters (∼36% for the distorted). Although these results demonstrate the importance of both, local distortions as well as nonlocal contributions to the damping anisotropy, they are not still able to reproduce the huge observed [10] maximum-minimum damping ratio.

We further proceed with our search for ingredients that could lead to a huge $\Delta\alpha_t$ by inspecting interface effects, which are present in thin films, grain boundaries, stacking faults, and materials in general. Such interfaces may influence observed properties, and in order to examine if they are relevant also for the reported alloys of Ref. [10], we considered these effects explicitly in the calculations. As a model interface, we considered a surface, what is, possibly, the most extreme case. Hence, we performed a set of α_t calculations for the $Fe_{50}Co_{50}(001)$, first on the VCA level. Analogous to the respective bulk systems, we found that the onsite contributions to the damping anisotropy are distinct, but they are not the main cause ($\Delta\alpha_{onsite} \sim 18\%$). However, the lack of inversion symmetry in this case gives a surprisingly large enhancement of $\Delta\alpha_t$, thus having its major contribution coming from the nonlocal damping terms, in particular from the next-nearest neighbors. Interestingly, negative nonlocal contributions appear when α_t is calculated in the [010] direction. These diminish the total damping (the onsite contribution being always positive) and gives rise to a larger anisotropy, as can be seen by comparison of the results shown in Table I and Supplemental Table S5. In this case, the total anisotropy was found to be more than ∼100% (corresponding to a maximum-minimum damping ratio larger than 200%).

A compilation of the most relevant theoretical results obtained here is shown in Fig. 2, together with the experimental data and the local density of states (LDOS) at E_F for each magnetization direction of a typical atom in the outermost layer (data shown in yellow). As shown in Fig. 2, the angular variation of α_t has a fourfold (C_{4v}) symmetry, with the smallest Gilbert damping occurring at 90° from the reference axis ([100], $\theta_H = 0°$) for both surface and bulk calculations. This

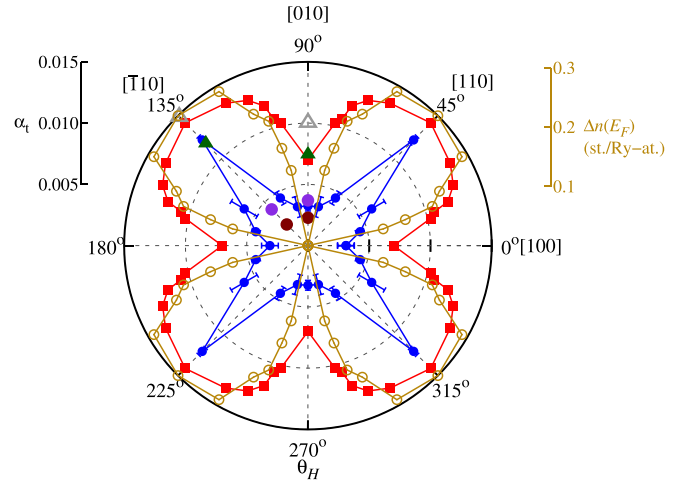FIG. 2. Total damping and LDOS difference at E_F, $\Delta n(E_F)$, as a function of θ_H, the angle between the magnetization direction and the [100] axis. Squares: (Red full) VCA $Fe_{50}Co_{50}(001)$ bcc. Triangles: (Green full) Average over 32 clusters (16 Fe-centered and 16 Co-centered), with bcc structure at the surface layers (Supplemental Material) embedded in a VCA medium; (gray open) similar calculations, but with a local lattice distortion. Circles: (Yellow open) $\Delta n(E_F)$ between $\theta_H = 0°$ and the current angle for a typical atom in the outermost layer of VCA $Fe_{50}Co_{50}(001)$ bcc, (blue full) experimental data [10] for a 10-nm $Fe_{50}Co_{50}/Pt$ thin film, (purple full) average bulk VCA $Fe_{50}Co_{50}$ bcc, and (brown full) the B2-FeCo bulk. Lines are guides for the eyes.

pattern, also found experimentally in [10], matches the in-plane bcc crystallographic symmetry and coincides with other manifestations of SOC, such as the anisotropic magnetoresistance [10,21]. Following the simplified Kambersky's formula [12,22], in which (see Supplemental Material) $\alpha \propto n(E_F)$ and, therefore, $\Delta\alpha \propto \Delta n(E_F)$, we can ascribe part of the large anisotropy of the FeCo alloys to the enhanced LDOS differences at the Fermi level, evidenced by the close correlation between $\Delta n(E_F)$ and $\Delta\alpha_t$ demonstrated in Fig. 2. Thus, as a manifestation of interfacial SOC (the so-called proximity effect [23]), the existence of $\Delta\alpha_t$ can be understood in terms of Rashba-like SOC, which has been shown to play an important role on damping anisotropy [24,25]. Analogous to the bulk case, the higher m_{orb} occurs where the system presents the smallest α_t, and the orbital moment anisotropy matches the $\Delta\alpha_t$ fourfold symmetry with a 90° rotation phase (see Supplemental Fig. S3). Note that a lower damping anisotropy than $Co_{50}Fe_{50}(001)$ is found for a pure Fe(001) bcc surface, where it is ∼49% (Supplemental Table S2), in accordance with Refs. [7,26], with a dominant contribution from the on-site damping values (conductivity-like character on the reciprocal space [19,27]).

The VCA surface calculations on real space allows to investigate the layer-by-layer contributions (intralayer damping calculation), as shown in Table I. We find that the major contribution to the damping surface anisotropy comes from the outermost layer, mainly from the difference in the minority 3d states around E_F. The deeper layers exhibit an almost oscillatory $\Delta\alpha_t$ behavior, similar to the oscillation mentioned in Ref. [28] and to the Friedel oscillations obtained for magnetic moments. The damping contributions from deeper layers are

much less influenced by the inversion symmetry breaking (at the surface), as expected, and eventually approaches the typical bulk limit. Therefore, changes in the electronic structure considered not only the LDOS of the outermost layer but also a summation of the LDOS of all layers (including the deeper ones), which produces an almost vanishing difference between $\theta_H = 0°$ and $\theta_H = 45°$ (also approaching the bulk limit). The damping anisotropy arising as a surface effect agrees with what was observed in the case of Fe [7] and CoFeB [29] on GaAs(001), where the damping anisotropy diminishes as the film thickness increases.

We also studied the impact of bct-like distortions *in* the surface, initially by considering the VCA model. Similar to the bulk case, tetragonal distortions may be important for the damping anisotropy at the surface, e.g., when local structural defects are present. Therefore, localized bct-like distortions of the VCA medium in the surface, particularly involving the most external layer, were investigated. The structural model was similar to what was used for the $Fe_{50}Co_{50}$ bulk, considering $\frac{c}{a} = 1.09$ (see Supplemental Material). Our calculations show that tetragonal relaxations around a typical site in the surface induce a $\Delta\alpha_t \sim 75\%$, from $\alpha_t^{[010]} = 8.94 \times 10^{-3}$ to $\alpha_t^{[110]} = 15.68 \times 10^{-3}$. The main effect of these distortions is an enhancement of the absolute damping values in each direction with respect to the pristine (bcc) system. This is due to an increase on α_{onsite}, from $\alpha_{\mathrm{onsite}}^{[010]} = 7.4 \times 10^{-3}$ to $\alpha_{\mathrm{onsite}}^{[010]} = 9.5 \times 10^{-3}$ and from $\alpha_{\mathrm{onsite}}^{[110]} = 8.7 \times 10^{-3}$ to $\alpha_{\mathrm{onsite}}^{[110]} = 11.7 \times 10^{-3}$; the resulting nonlocal contributions remain similar to the undistorted case. The influence of bct-like distortions on the large damping value in the $Fe_{50}Co_{50}$ surface is in line with results of Mandal *et al.* [30] and is related to the transition of minority spin electrons around E_F.

We then considered explicit 10-atom $Fe_{50}Co_{50}$ clusters embedded in a VCA FeCo surface matrix. The results from these calculations were obtained as an average over 16 Fe-centered and 16 Co-centered clusters. We considered clusters with undistorted bcc crystal structure (Fig. 2, green full triangles) as well as clusters with local tetragonal distortions (Fig. 2, gray open triangles). As shown in Fig. 2 the explicit local tetragonal distortion influences the damping values ($\alpha_t^{[010]} = 10.03 \times 10^{-3}$ and $\alpha_t^{[110]} = 14.86 \times 10^{-3}$) and the anisotropy, but not enough to reproduce the huge values reported in the experiments.

A summary of the results obtained for each undistorted FeCo cluster at the surface is shown in Fig. 3: Co-centered clusters in Fig. 3(a) and Fe-centered clusters in Fig. 3(b). A large variation of α_t values is seen from cluster to cluster, depending on the spatial distribution of atomic species. It is clear that α_t is larger when there is a larger number of Fe atoms in the surface layer that surrounds the central, reference cluster site. This correlation can be seen by the numbers in parenthesis on top of the blue symbols (total damping for each of the 16 clusters that were considered) in Fig. 3. We also notice from the figure that the damping in Fe-centered clusters is lower than in Co-centered clusters and that the [010] magnetization direction always exhibits lower values. In the Fig. 3 inset, the onsite contributions to the damping, α_{onsite} and the LDOS at E_F in the central site of each cluster are shown: A correlation, where both trends are the same, can be observed.

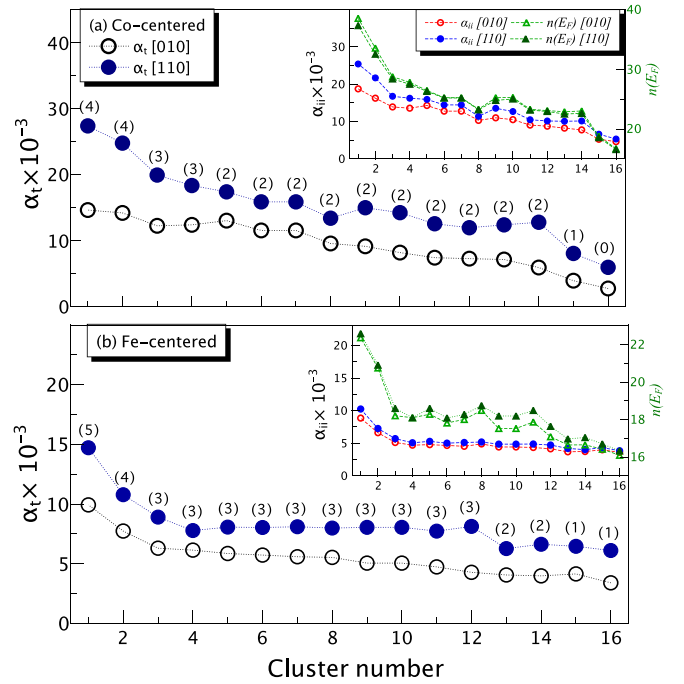FIG. 3. Damping for the [010] (open circles) and [110] (full circles) magnetization directions for distinct types of 10-atom $Fe_{50}Co_{50}$ bcc clusters, embedded in VCA $Fe_{50}Co_{50}$(001) bcc and without any distortion around the reference atom (for which α_t and α_{onsite} are shown). (a) Co-centered and (b) Fe-centered clusters. The quantity of Fe atoms in the surface layers (near vacuum) are indicated by the numbers in parenthesis and the results have been ordered such that larger values are to the left in the plots. *Insets*: α_{onsite} for the [010] (red open circles) and [110] (blue filled circles) magnetization directions, and corresponding LDOS, $n(E_F)$, at the Fermi level (green filled and unfilled triangles) at the central atom (placed in the outermost layer) for both types of clusters. Lines are guides for eyes.

The results in Fig. 3 shows that the neighborhood influences not only the local electronic structure at the reference site [changing $n(E_F)$ and α_{onsite}] but also modifies the nonlocal damping α_{ij}, leading to the calculated α_t. In other words, the local spatial distribution affects how the total damping is manifested, something which is expressed differently among different clusters. This may open up for materials engineering of local and nonlocal contributions to the damping.

Conclusions. We demonstrate here that real-space electronic structure, based on density functional theory, yield a large Gilbert damping anisotropy in $Fe_{50}Co_{50}$ alloys. Theory leads to a large damping anisotropy, when the magnetization changes from the [010] to the [110] direction, which can be as high as ~100% (or 200% in the minimum-maximum damping ratio) when surface calculations are considered. This is in particular found for contributions from surface atoms in the outermost layer. Hence the results presented here represents one more example, in addition to the well-known enhanced surface orbital moment [31], of the so-called interfacial SOC. This damping anisotropy, which holds a bcc-like fourfold (C_{4v}) symmetry, has a close relation to the LDOS difference of the most external layer at E_F (majorly contributed by the minority *d* states), as well as to the orbital moment anisotropy with a 90° phase. As a distinct example of an interface, we

consider explicitly the $Fe_{50}Co_{50}$ cluster description of the alloy. In this case, besides an on-site contribution, we find that the damping anisotropy is mostly influenced by nonlocal next-nearest-neighbor interactions.

Several Gilbert damping anisotropy origins are also demonstrated here, primarily related to the presence of interfaces, alloy composition, and local structural distortions (as summarized in Supplemental Table S6 [32]). Primarily we find that: (i) the presence of Co introduces an enhanced spin-orbit interaction and can locally modify the nonlocal damping terms; (ii) the randomness of Co in the material can modestly increase $\Delta\alpha_t$ as a total effect by creating Co-concentrated clusters with enhanced damping; (iii) at the surface, the spatial distribution of Fe/Co, increases the damping when more Fe atoms are present in the outermost layer; and (iv) the existence of local, tetragonal distortions, which act in favor (via SOC) of the absolute damping enhancement by modifying the α_{onsite} of the reference atom and could locally change the spin relaxation time. Furthermore, in relationship to the work in Ref. [10], we show here that bulk-like tetragonal distortions, which in Ref. [10] were suggested to be the key reason behind the observed huge anisotropy of the damping, can in fact not explain the experimental data. Such distortions were explicitly considered here, using state-of-the-art theory, and we clearly demonstrate that this alone cannot account for the observations.

Although having a similar trend as the experimental results of Ref. [10], we do not reproduce the most extreme maximum-minimum ratio reported in the experiment, ∼400% (or $\Delta\alpha_t \sim$ 300%). The measured damping does, however, include effects beyond the intrinsic damping that is calculated from our electronic structure methodology. Other mechanisms are known to influence the damping parameter, such as contributions from eddy currents, spin-pumping, and magnon scattering, to name a few. Thus it is possible that a significant part of the measured anisotropy is caused by other, extrinsic, mechanisms. Despite reasons for differences between observation and experiment on films of $Fe_{50}Co_{50}$ alloys, the advancements presented here provide new insights on the intrinsic damping anisotropy mechanisms, something that is relevant for the design of new magnetic devices.

---

[1] O. Eriksson, A. Bergman, L. Bergqvist, and J. Hellsvik, *Atomistic Spin Dynamics: Foundations and Applications* (Oxford University Press, Oxford, 2017).

[2] K. Gilmore, Y. U. Idzerda, and M. D. Stiles, Phys. Rev. Lett. **99**, 027204 (2007).

[3] A. Brataas, A. D. Kent, and H. Ohno, Nat. Mater. **11**, 372 (2012).

[4] M. A. W. Schoen, D. Thonig, M. L. Schneider, T. J. Silva, H. T. Nembach, O. Eriksson, O. Karis, and J. M. Shaw, Nat. Phys. **12**, 839 (2016).

[5] D. Thonig, Y. Kvashnin, O. Eriksson, and M. Pereiro, Phys. Rev. Materials **2**, 013801 (2018).

[6] Y. Liu, Z. Yuan, R. J. H. Wesselink, A. A. Starikov, and P. J. Kelly, Phys. Rev. Lett. **113**, 207202 (2014).

[7] L. Chen, S. Mankovsky, S. Wimmer, M. Schoen, H. Körner, M. Kronseder, D. Schuh, D. Bougeard, H. Ebert, D. Weiss, and C. H. Back, Nat. Phys. **14**, 490 (2018).

[8] H. Ebert, D. Ködderitzsch, and J. Minár, Reports Prog. Phys. **74**, 096501 (2011).

[9] A. J. Lee, J. T. Brangham, Y. Cheng, S. P. White, W. T. Ruane, B. D. Esser, D. W. McComb, P. C. Hammel, and F. Yang, Nat. Commun. **8**, 234 (2017).

[10] Y. Li, F. Zeng, S. S.-L. Zhang, H. Shin, H. Saglam, V. Karakas, O. Ozatay, J. E. Pearson, O. G. Heinonen, Y. Wu, A. Hoffmann, and W. Zhang, Phys. Rev. Lett. **122**, 117203 (2019).

[11] S. Mankovsky, D. Ködderitzsch, G. Woltersdorf, and H. Ebert, Phys. Rev. B **87**, 014430 (2013).

[12] V. Kamberský, Can. J. Phys. **48**, 2906 (1970).

[13] V. Kamberský, Czech. J. Phys. **26**, 1366 (1976).

[14] S. Mankovsky, S. Wimmer, and H. Ebert, Phys. Rev. B **98**, 104406 (2018).

[15] S. Frota-Pessôa, Phys. Rev. B **46**, 14570 (1992).

[16] S. Frota-Pessôa, A. B. Klautau, and S. B. Legoas, Phys. Rev. B **66**, 132416 (2002).

[17] U. von Barth and L. Hedin, J. Phys. C: Solid State Phys. **5**, 1629 (1972).

[18] D. C. M. Rodrigues, A. B. Klautau, A. Edström, J. Rusz, L. Nordström, M. Pereiro, B. Hjörvarsson, and O. Eriksson, Phys. Rev. B **97**, 224402 (2018).

[19] K. Gilmore, M. D. Stiles, J. Seib, D. Steiauf, and M. Fähnle, Phys. Rev. B **81**, 174414 (2010).

[20] S. S. A. Razee, J. B. Staunton, B. Ginatempo, F. J. Pinski, and E. Bruno, Phys. Rev. Lett. **82**, 5369 (1999).

[21] J. Moser, A. Matos-Abiague, D. Schuh, W. Wegscheider, J. Fabian, and D. Weiss, Phys. Rev. Lett. **99**, 056601 (2007).

[22] M. Oogane, T. Kubota, H. Naganuma, and Y. Ando, J. Phys. D: Appl. Phys. **48**, 164012 (2015).

[23] I. Žutić, A. Matos-Abiague, B. Scharf, H. Dery, and K. Belashchenko, Mater. Today **22**, 85 (2019).

[24] J.-V. Kim, Phys. Rev. B **92**, 014418 (2015).

[25] C. A. Akosa, A. Takeuchi, Z. Yuan, and G. Tatara, Phys. Rev. B **98**, 184424 (2018).

[26] W. Zhang, Y. Li, N. Li, Y. Li, Z.-z. Gong, X. Yang, Z.-k. Xie, R. Sun, X.-q. Zhang, W. He, and Z.-h. Cheng, J. Magn. Magn. Mater. **496**, 165950 (2020).

[27] B. Khodadadi, A. Rai, A. Sapkota, A. Srivastava, B. Nepal, Y. Lim, D. A. Smith, C. Mewes, S. Budhathoki, A. J. Hauser *et al.*, Phys. Rev. Lett. **124**, 157201 (2020).

[28] D. Thonig and J. Henk, New J. Phys. **16**, 013032 (2014).

[29] H. Tu, J. Wang, Z. Huang, Y. Zhai, Z. Zhu, Z. Zhang, J. Qu, R. Zheng, Y. Yuan, R. Liu *et al.*, J. Phys.: Condens. Matter **32**, 335804 (2020).

[30] R. Mandal, J. Jung, K. Masuda, Y. Takahashi, Y. Sakuraba, S. Kasai, Y. Miura, T. Ohkubo, and K. Hono, Appl. Phys. Lett. **113**, 232406 (2018).

[31] M. Tischer, O. Hjortstam, D. Arvanitis, J. H. Dunn, F. May, K. Baberschke, J. Trygg, J. M. Wills, B. Johansson, and O. Eriksson, Phys. Rev. Lett. **75**, 1602 (1995).

[32] See Supplemental Material at http://link.aps.org/supplemental/10.1103/PhysRevB.103.L220405 for a detailed description of the theory, damping comparison with literature, damping anisotropy values, and LDOS, which includes Refs. [2,4,5,7,10,11,13,15,17,19,22,26–28,30,33–64].

[33] O. K. Andersen, Phys. Rev. B **12**, 3060 (1975).

[34] R. Meckenstock, D. Spoddig, Z. Frait, V. Kambersky, and J. Pelzl, J. Magn. Magn. Mater. **272**, 1203 (2004).

[35] Y. O. Kvashnin, R. Cardias, A. Szilva, I. Di Marco, M. I. Katsnelson, A. I. Lichtenstein, L. Nordström, A. B. Klautau, and O. Eriksson, Phys. Rev. Lett. **116**, 217202 (2016).

[36] D. C. M. Rodrigues, A. Szilva, A. B. Klautau, A. Bergman, O. Eriksson, and C. Etz, Phys. Rev. B **94**, 014413 (2016).

[37] S. B. Legoas, A. A. Araujo, B. Laks, A. B. Klautau, and S. Frota-Pessôa, Phys. Rev. B **61**, 10417 (2000).

[38] S. Frota-Pessôa, L. A. de Mello, H. M. Petrilli, and A. B. Klautau, Phys. Rev. Lett. **71**, 4206 (1993).

[39] A. B. Klautau and S. Frota-Pessôa, Phys. Rev. B **70**, 193407 (2004).

[40] A. Bergman, L. Nordström, A. B. Klautau, S. Frota-Pessôa, and O. Eriksson, Surf. Sci. **600**, 4838 (2006).

[41] M. M. Bezerra-Neto, M. S. Ribeiro, B. Sanyal, A. Bergman, R. B. Muniz, O. Eriksson, and A. B. Klautau, Sci. Rep. **3**, 3054 (2013).

[42] R. Cardias, M. M. Bezerra-Neto, M. S. Ribeiro, A. Bergman, A. Szilva, O. Eriksson, and A. B. Klautau, Phys. Rev. B **93**, 014438 (2016).

[43] O. K. Andersen, O. Jepsen, and D. Glötzel, in *Highlights of Condensed-Matter Theory*, edited by F. Bassani, F. Fumi, and M. P. Tosi (North Holland, Amsterdam, 1985).

[44] R. Haydock, in *Solid State Physics*, edited by H. Ehrenreich, F. Seitz, and D. Turnbull (Academic Press, New York, 1980).

[45] S. Frota-Pessôa, Phys. Rev. B **69**, 104401 (2004).

[46] A. B. Klautau and S. Frota-Pessôa, Surf. Sci. **579**, 27 (2005).

[47] N. Beer and D. G. Pettifor, in *The Electronic Structure of Complex Systems*, edited by W. Temmermann and P. Phariseau (Plenum Press, New York, 1984).

[48] K. Shikada, M. Ohtake, F. Kirino, and M. Futamoto, J. Appl. Phys. **105**, 07C303 (2009).

[49] I. Turek, J. Kudrnovský, and V. Drchal, Phys. Rev. B **92**, 214407 (2015).

[50] H. Ebert, S. Mankovsky, D. Ködderitzsch, and P. J. Kelly, Phys. Rev. Lett. **107**, 066603 (2011).

[51] R. Chimata, E. K. Delczeg-Czirjak, A. Szilva, R. Cardias, Y. O. Kvashnin, M. Pereiro, S. Mankovsky, H. Ebert, D. Thonig, B. Sanyal, A. B. Klautau, and O. Eriksson, Phys. Rev. B **95**, 214417 (2017).

[52] E. Barati, M. Cinal, D. M. Edwards, and A. Umerski, Phys. Rev. B **90**, 014420 (2014).

[53] M. Oogane, T. Wakitani, S. Yakata, R. Yilgin, Y. Ando, A. Sakuma, and T. Miyazaki, Jpn. J. Appl. Phys. **45**, 3889 (2006).

[54] C. Vittoria, S. D. Yoon, and A. Widom, Phys. Rev. B **81**, 014412 (2010).

[55] R. Weber, D.-S. Han, I. Boventer, S. Jaiswal, R. Lebrun, G. Jakob, and M. Kläui, J. Phys. D: Appl. Phys. **52**, 325001 (2019).

[56] N. Umetsu, D. Miura, and A. Sakuma, J. Phys. Soc. Jpn. **81**, 114716 (2012).

[57] M. A. W. Schoen, J. Lucassen, H. T. Nembach, T. J. Silva, B. Koopmans, C. H. Back, and J. M. Shaw, Phys. Rev. B **95**, 134410 (2017).

[58] M. Acet, C. John, and E. Wassermann, J. Appl. Phys. **70**, 6556 (1991).

[59] J. M. Shaw, H. T. Nembach, and T. J. Silva, Appl. Phys. Lett. **99**, 012503 (2011).

[60] T. Seki, J. Shimada, S. Iihama, M. Tsujikawa, T. Koganezawa, A. Shioda, T. Tashiro, W. Zhou, S. Mizukami, M. Shirai, and K. Takanashi, J. Phys. Soc. Jpn. **86**, 074710 (2017).

[61] M. Arora, C. Fowley, T. McKinnon, E. Kowalska, V. Sluka, A. M. Deac, B. Heinrich, and E. Girt, IEEE Magn. Lett. **8**, 1 (2016).

[62] N. Romming, C. Hanneken, M. Menzel, J. E. Bickel, B. Wolter, K. von Bergmann, A. Kubetzka, and R. Wiesendanger, Science **341**, 636 (2013).

[63] L. V. Dzemiantsova, M. Hortamani, C. Hanneken, A. Kubetzka, K. von Bergmann, and R. Wiesendanger, Phys. Rev. B **86**, 094427 (2012).

[64] C. Kittel, Phys. Rev. **76**, 743 (1949).